ACS MATERIALS LETTERS

www.acsmaterialsletters.org
Letter

Liquid Surface Synthesis of Ultrathin Two-Dimensional Metal Halide Perovskite

Jiaxiong Li, Mordechai Kot, Nina Cielica, Jacopo Pinna, Lijun Chen, Francesco Modena, Laurence Lutsen, Wouter T. M. Van Gompel, and Maria Antonietta Loi*

Cite This: https://doi.org/10.1021/acsmaterialslett.5c01358
Read Online

ABSTRACT: Two-dimensional (2D) metal halide perovskite-like quantum wells can be obtained by slicing the inorganic perovskite lattices with large organic molecules, where the number of consecutive inorganic slabs (n) determines the quantum confinement. Synthesizing large-area and ultrathin 2D perovskite sheets is crucial to achieving heterostructures for future thin-sheet optoelectronic devices. In this work, we demonstrate a synthesis method in which perovskite precursor solutions are introduced on an antisolvent liquid surface. Well-defined n = 1 sheets with sub-10 nm thickness and up to 50 μm lateral size are obtained in a scalable manner. This is achieved through careful engineering of subphase and spreading phase compositions to encourage controlled perovskite crystallization at the antisolvent−air interface. Structural and spectroscopic characterizations reveal a high phase purity and a clean excitonic emission, with their overall optical properties comparable to those of the highly crystalline films fabricated by blade coating, highlighting the clear potential of this liquid surface synthesis strategy.

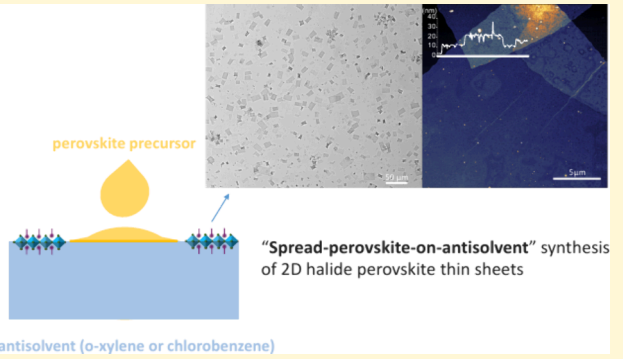

Metal halide perovskites,[1] marked by their facile solution-based synthesis and flexible chemical design, have occupied in the last 12 years a major share of the attention of researchers interested in optoelectronics.[2,3] Most recently, next to the three-dimensional (3D) lattices belonging to the metal halide perovskite family, their two-dimensional (2D) homologues obtained by inserting large organic spacer molecules that break the 3D lattice into 2D perovskite-like slabs have also entered the optoelectronic arena, mostly because of their excitonic properties and fine control over the confinement degree.[4−6] Inserting monofunctional spacers along the ⟨100⟩ planes could yield the staggered slab arrangement or the so-called Ruddlesden−Popper (RP) phases with a general formulation of $A'_2A_{n-1}B_nX_{3n+1}$, where A is a small cation, A′ is large spacer molecule, B is a metal cation in the octahedron center, and X is a halogen anion. These material systems can crucially be characterized by the number of corner-sharing inorganic layers (n) hosting small A-site cations between the spacer interruptions in (00l) directions, a parameter that determines the quantum well properties (Figure 1a, top shows the case for n = 1, 2, and 3, respectively). This quantum confinement can, to an extent, be preserved regardless of the material's physical thickness, as the film can be viewed as a periodic arrangement of the "well" and the "barrier".

Modern optoelectronics is deeply rooted in the ability to fabricate heterostructures of different semiconductors with the aim of directing carriers to specific regions of a device to favor charge recombination or separation. Traditionally, semiconductor heterostructures are fabricated by epitaxially growing different materials on top of each other, where the lattice matching represents a strong limitation for the materials that can be used.[7] In recent years, increased interest has also appeared in the fabrication of heterostructures that are not limited by lattice mismatch. While common examples are definitely the transition metal dichalcogenides and organic semiconductor heterostructure,[8,9] there is also a growing desire to form heterostructures using the soft RP perovskite phases with different bandgap, which could be simply obtained via altering halide compositions or n values.[10] For standard thin film fabrication techniques, there are however major bottlenecks for the sequential deposition of perovskite layers: (1) due to the highly dynamic and ionic nature of the halide perovskite lattice, deposition of heterolayers from solution or vapor could be destructive; (2) for n > 1 quasi-2D perovskites, chemical disproportionation would cause the formation of mixed-n phases with unwanted physical properties.[11,12] This seems to be different from transition metal dichalcogenides, where the so-called van der Waals assembly of these 2D

Received: October 7, 2025
Revised: December 8, 2025
Accepted: December 9, 2025

https://doi.org/10.1021/acsmaterialslett.5c01358
ACS Materials Lett. XXXX, XXX, XXX−XXX

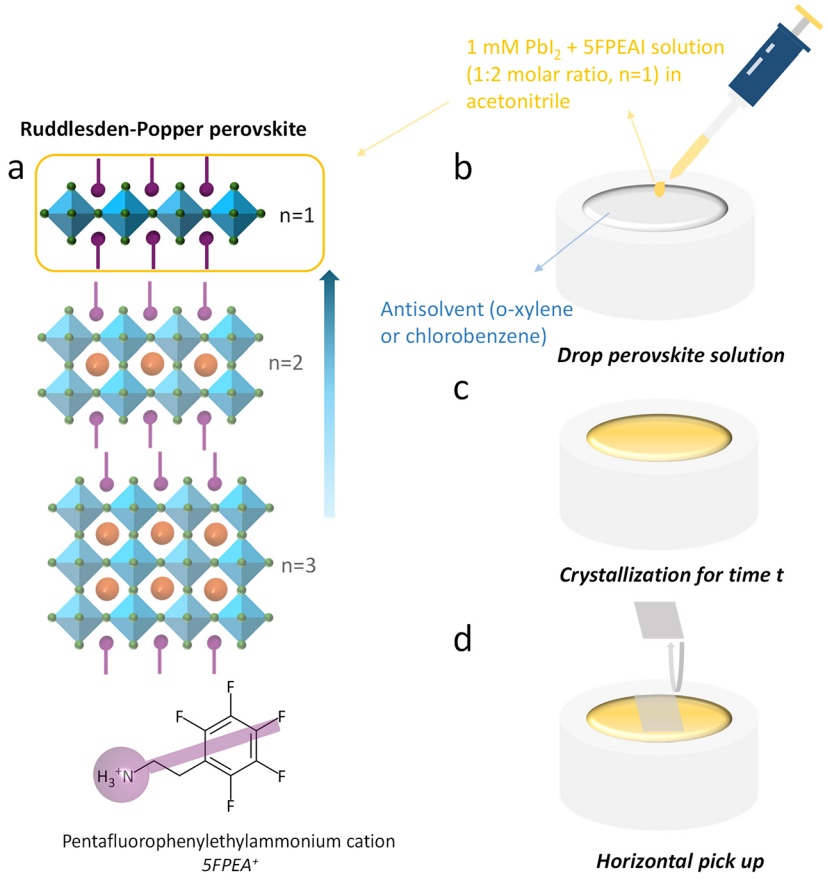

Figure 1. (a) Top: schematic representation of Ruddlesden−Popper 2D metal halide perovskite phases, which achieve quantum confinement in ⟨100⟩ planes using large spacer molecules. Blue octahedra: $[BX_6]$ inorganic cages; green spheres: halide anions; red spheres: small A-site cations; purple ball-and-sticks: large spacer molecules forcing inorganic slab openings; *n*: number of consecutive inorganic layers between organic spacers. Bottom: chemical structure of the spacer 2,3,4,5,6-pentafluorophenethylammonium cation ($5FPEA^+$). (b−d) Process flow of the proposed "spread-perovskite-on-antisolvent" method: (b) $n = 1$ perovskite precursor solution (PbI_2:5FPEAI = 1:2) is introduced dropwise on an antisolvent substrate. (c) Perovskite crystallization is allowed for time *t*, before (d) sample pickup by horizontal contact using a solid substrate and drying in a vacuum.

materials is a major research topic leading to the discovery of interesting physical phenomena.[13,14] Taking inspiration from this, heterojunctions made of prefabricated ultrathin perovskite sheets with controlled layer numbers and phase purity have been demonstrated.[15] Potentially, these systems will be interesting for the fabrication of a device devoted to artificial lighting and light detection,[16] while the key challenge here is how to obtain high quality 2D perovskite thin sheets with a large lateral dimension.

Several authors have reported liquid phase synthesis of perovskite thin sheets, while each of these methods still faces specific challenges in either scaling up or composition control. We supply some details of these methods in Scheme S1 and Supplementary Note 1. Crucially, Dou et al.[17] showed early on that drying a droplet of $n = 1$ perovskite solution, which requires careful solvent engineering, on a solid surface can yield ∼5 μm lateral single-layer sheets ("droplet", Scheme S1a). Jin's group[18,19] instead utilized solution surface crystallization from a *droplet of perovskite solution* upon proper solvent selection and temperature control ("droplet surface", Scheme S1c). This enabled the growth of >100 μm lateral-sized crystals with nm-scale thickness, which are transferred via stamping. Utilizing the solution−air interface, a large open surface of *perovskite solutions* ("bulk surface", Scheme S1e) has also supported surface-initiated single crystal growth, where the involvement of liquid surface energy in the crystallization process has been discussed.[20,21] However, in this case, it is extremely challenging to maintain the nanometer-level thickness in obtained crystals. To limit *z*-direction crystal growth at the liquid−air interface, Langmuir-film-inspired techniques are highly suitable. Era's group has demonstrated that spreading long chain alkyl ammonium spacers on *metal halide solutions* induces the formation of $n = 1$ halide perovskite Langmuir films ("spread spacer", Scheme S1g); however, obtaining higher *n* value perovskites would not be feasible using this method.

Facing these issues, here we report a facile "*spread-perovskite-on-antisolvent*" method to prepare large-sized high-quality $n = 1$ metal halide perovskite thin sheets in large quantities. This method is able to utilize a large surface area of the liquid substrate and has the potential for fabricating phase-pure higher *n* value perovskite nanosheets, since the perovskite precursors are contained entirely in the spreading solution. We show that, through careful selection of antisolvent substrate and perovskite precursor solution, 2D perovskite sheets of ∼50 μm lateral size and <10 nm thickness could be obtained in a scalable manner. Microscopic, structural and optical characterizations of the synthesized perovskite sheets showcase their phase purity and narrow excitonic emission benchmarked by high-quality blade-coated perovskite thin films.

https://doi.org/10.1021/acsmaterialslett.5c01358
ACS Materials Lett. XXXX, XXX, XXX−XXX

In our "*spread-perovskite-on-antisolvent*" method, a spreading phase composed of dilute perovskite precursor solution of n = 1 stoichiometry is spread on an antisolvent liquid substrate, on which surface the nucleation and growth of thin perovskite sheets take place. For optimal anchoring and spreading at the antisolvent−air interface, a perfluorinated spacer molecule 2,3,4,5,6-pentafluorophenethylammonium (5FPEA$^+$, Figure 1a, bottom) is used to achieve the composition of $(5FPEA)_2PbI_4$, which was found to be more suitable in the synthesis compared to its nonfluorinated counterpart PEA_2PbI_4 (*vide infra*), likely due to the very low surface energy of the perfluoro spacer molecules.

In a typical experiment, 50 μL of $(5FPEA)_2PbI_4$ solution in acetonitrile is spread dropwise in a bolting pattern on the liquid substrate (o-xylene or chlorobenzene) contained in a circular Teflon bath (Ø30 mm) (Figure 1b). The crystallization at room temperature is allowed for a period (in minutes), where yellow precipitates gradually form and diffuse on the surface (Figure 1c). After that, samples are picked up with Si, quartz (10 × 10 mm^2) or metal grids for electron microscopy in parallel contact (Langmuir−Shaefer method) and dried in a vacuum at room temperature (Figure 1d).

We begin with the selection of the spreading phase and subphase solvents. For the spreading phase, only a handful of solvents present good solubility for lead halide perovskites.[22,23] Considering that the solvent should have a lower density and a lower surface energy than the subphase, and be easily removable,[24] acetonitrile (MeCN, 0.79 g/cm^3, 19.10 mN/m @20 °C, bp 82 °C) was selected, as in the *droplet* on solid surfaces method (Scheme S1a).[17]

For the subphase, several considerations are necessary. First, it should have a relatively low solubility for lead halide perovskite precursors to trigger crystallization. This is a rather complex chemical environment for the perovskite precursors as the antisolvent, solvent, and solute all interact with each other during the one-step synthesis. It was found that spreading perovskite solution on strong antisolvents (e.g., toluene) results in quick agglomeration, while the slightly better solubilities seen in some solvents,[22] that either offer coordination (e.g., cyclohexanone) to Pb^{2+} or hydrogen bonding (e.g., isopropanol) to spacer cations or I^-, result in undesired full solvation of the perovskite precursor. Second, the subphase should possess a large density as well as a high liquid−air surface energy to enhance the tendency of the dropped solution to spread and of the crystals to stay on the liquid surface. This alone, however, is not sufficient to guarantee a good synthesis, as in the case for iodobenzene (1.83 g/cm^3, 39.38 mN/m @20 °C), where while the spreading phase disperses extremely well, the synthesized crystals show small size (~μm), large thickness (~30 nm), and porous morphology (Figure S1a). This may be due to the halogen−halogen interactions between the subphase and perovskite chemistry (lead iodide octahedra), again stressing the importance of chemical interactions. Finally, regarding the miscibility of spreading phase and subphase solvents, it has been shown that, with proper solutes, miscible solvents could also allow Langmuir film formation.[25,26] After trials with various antisolvent systems, o-xylene (OX, 0.88 g/cm^3, 30.10 mN/m @20 °C) and chlorobenzene (CB, 1.11 g/cm^3, 33.60 mN/m @20 °C) stood out as the best candidates for our approach, despite both being miscible with MeCN.

The initial concentration of the spreading phase precursor solution was set to 1 mM. A few sheets with lateral dimensions on the 10s of μm and thickness below 10 nm were obtained after picking up with a Si substrate (Figure S1b), while most of the substrate surface is populated by 3D crystal agglomerates. This is especially notable for the case of nonfluorinated chemistry PEA_2PbI_4 (Figure S1c). Also noted are the clustered small and porous sheets formed after a short growing time (2 min on CB, Figure S2a), and large and thick stars were obtained after waiting longer before pickup (5 min on CB, Figure S2b). This signifies unfavorable crystallization kinetics under the current parameters, which exhibit rapid perovskite nucleation and uncontrolled growth in the z direction.

This crystallization kinetic problem was systematically tackled through engineering of the spreading phase composition. First, before making the final MeCN solution, the precursor was predissolved into a 1 M dimethylformamide (DMF) solution, to slow down the rapid crystallization (especially in z) when the solute is put into contact with the antisolvent. Second, the final concentration of the spreading phase in MeCN was optimized. The 1 M DMF stock solution was diluted to x M in DMF and then to y mM in MeCN, yielding the solution formulation "xDMF yMeCN".

The effect of introducing DMF as a presolvent can be found when comparing Figures S3 and S4 (spread on OX) but is especially obvious in Figure S5 (spread on CB). For the same final concentration, additional DMF (up to 10x dilution to reach 0.1DMF) reduces the growth rate and allows better 2D sheet formation. However, the use of DMF is to be balanced, as it possesses both a high density (0.94 g/cm^3) and a high surface energy (37.10 mN/m @20 °C). In addition, the removal of DMF from the synthesized perovskite is nontrivial due to its high bp (153 °C) and strong coordination with lead complexes.

When the final precursor solution concentration is increased, faster nucleation and growth are observed, producing a larger quantity of sheets after the same growth time. Up to 8 mM, increasing concentration did not lead to notable adverse effects, while agglomeration and thick crystals started to show earlier in CB (Figure S5). The samples from different growing times are compared; it is reasonable to assume the presence of Ostwald ripening, as longer-waited samples present larger but fewer 2D perovskite sheets. In fact, in Scanning Transmission Electron Microscopy (STEM) micrographs, we observe crystals possibly in the process of assembling into a larger entity (Figure S6).

After the process optimization, the liquid surface synthesized samples were studied by using microscopic characterization tools. In Figure 2a, on a quartz substrate a high population density of perovskite sheets with rather uniform thickness and lateral size (approaching 50 μm) is observed from the Bright-Field Optical Microscope (OM) micrograph. In some regions, we can also see clean overlaps between the stacked sheets. The Scanning Electron Microscope (SEM) micrograph (Figure S7) also shows sheets piling up on the "coffee ring" region on the substrate, suggesting that further substrate treatments may allow higher utilization of the liquid surface grown crystals.[27] For a closer look at the harvested sheets, the STEM micrograph (Figure 2b) shows one large sheet of ~25 nm thickness and ~40 μm lateral dimension where a relatively dense surface texture can be observed against the amorphous carbon background. In the Atomic Force Microscopy (AFM) measurement (Figure 2c, also see further examples in Figure S8), several cracks and various surface contaminations (including occasional particle inclusions) are visible. Still, the

https://doi.org/10.1021/acsmaterialslett.5c01358
ACS Materials Lett. XXXX, XXX, XXX−XXX

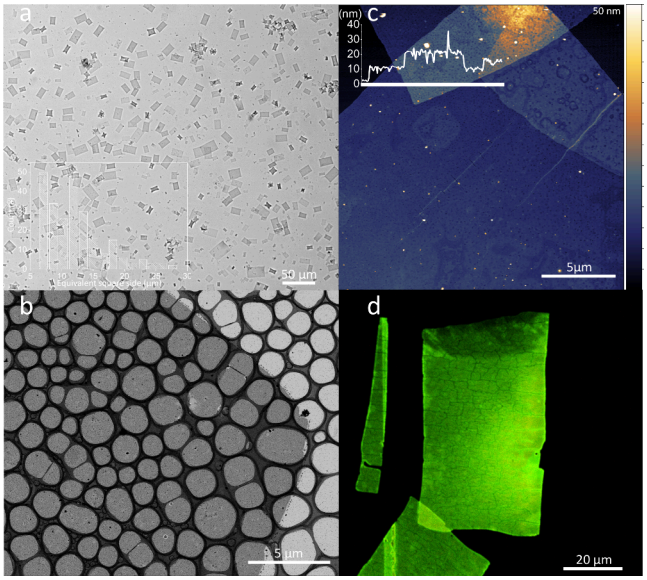

Figure 2. Microscopic characterizations of liquid surface grown $(5FPEA)_2PbI_4$ sheets. (a) Transmission Bright-Field Optical Microscope (OM) micrograph showcasing the quantity of obtained perovskite sheets with the inset showing statistics of equivalent sheet sizes. (b) Bright Field Scanning Transmission Electron Microscope (STEM) micrograph on a TEM grid with amorphous carbon supporting film, showing the edges of a $(5FPEA)_2PbI_4$ sheet. (c) Atomic Force Microscope (AFM) image and (d) photoluminescence (PL) Confocal Microscope image of stacked $(5FPEA)_2PbI_4$ sheets. Sample fabrication parameters: (a) 0.2DMF 8MeCN solution spread on o-xylene and pickup after wait time of 1 min; (b–d) 0.2DMF 4MeCN soulution spread on o-xylene and pickup after wait time of 2 min.

body of the sheets is flat and uniform in ∼10 nm thickness (∼5 octahedra layers). This is especially clear from the overlapping region of three stacked sheets, where the line profile identifies the individual sharp edges of these 2D materials. From the confocal photoluminescence (PL) microscope micrographs (Figure 2d), the sheets emit homogeneously in the 515 ± 30 nm window, agreeing with the characteristics of a n = 1 lead iodide-based perovskite. The confocal micrograph also clearly shows the surface textures and presence of cracks. When the confocal micrographs are compared with OM images, it is apparent that thinner sheets could not be detected in PL.

To balance the yield and geometry of formed perovskite thin sheets, the samples made by recipe 0.2DMF 4MeCN spread on OX for 2 min were selected for further investigations. The crystal structure of these liquid surface grown perovskite sheets (LS) was provided by powder X-ray diffraction (XRD). In Figure 3a, the diffraction pattern presents clear Bragg peaks that are equally spaced and can be indexed with (00l) Miller indexes. These features are typical of n = 1 ⟨100⟩ 2D perovskites with inorganic sublattice planes parallel to the substrate.[28−31] From the previously obtained crystal structure of $(5FPEA)_2PbI_4$ single crystal,[31] we also supply the simulated XRD pattern which shows good agreements with our data. The signal-to-noise ratio is relatively low, likely due to sample quantity, yet the 2D sheets did not present notable features of other phases. From the (002) Bragg peak, the d_{002} interplanar distance was determined to be 17.2 Å, in trend with reports on 2D PEA perovskites[28] and in agreement with the increased spacings when using their monofluorinated (14.29 → 14.52 Å from PEA to 3-FPEA)[32] and penta-fluorinated analogues (17.47−17.50 Å for $(5FPEA)_2SnI_4$).[33,34] Debye−Scherrer analysis revealed an average crystallite size of 60 nm, indicating the average thickness of the perovskite sheets under detection.

To benchmark the crystal quality of the LS sample, we fabricated $(5FPEA)_2PbI_4$ perovskite thin films by blade coating (BC) from DMF solution with 10% dimethyl sulfoxide; see the Experimental Section in the Supporting Information for details. The powder XRD pattern obtained from these thin films (Figure 3b) displays the same (00l) Bragg peak series with d_{002} = 17.6 Å, with a crystallite size of 95 nm. The crystal structures of LS and BC were thus analogous barring the thickness differences, which for the latter depend on BC parameters.

With the stronger signal in BC, we also observed a set of much fainter equally spaced Bragg peaks (see the inset of the logarithmic plot). This points to a spurious 2D phase with increased interlayer separation (19.5 Å), which might be due to trapped DMF solvent, even with both deposition and annealing done at 110 °C. The specific interlayer separation of this phase in fact falls into the category of solvent intercalated 2D halide perovskites.[33] In addition, 1D perovskite phases that are difficult to avoid for solution deposited and annealed 2D perovskite films could also have been a culprit for the peak at 2θ = ∼8°.[35,36] These impurities overall represent only a tiny volumetric fraction in BC, but nevertheless, there is no signature of solvent intercalation in LS (synthesized at room temperature). Obviously, this observation may be affected by the poorer signal-to-noise ratio of the LS XRD result, but on the other hand, the limited use of DMF during the LS fabrication may determine its phase purity.

We conducted further optical measurements on the LS and BC samples. The absorbance spectra of these two samples can be found in Figure 3c, where the excitonic peak appeared at 500 nm for BC sample and 502 nm for LS sample, and the absorption stairs representing 2D electron states can be identified. In the Raman spectra (Figure 3d), strong peaks at 44 and 58 cm^{-1} (5.48 and 7.24 meV, respectively) are present in both samples which represent the signatures of the inorganic cages of 2D perovskite.[37] As from the XRD results, LS and BC behave in the same way as typical n = 1 lead iodide perovskites.

Temperature-dependent and time-resolved PL measurements further provided valuable information about the optical properties and therefore the quality of the samples. Figure 4a shows the steady-state PL spectra at room temperature (light) and 4.3 K (dark color). At room temperature, the narrow emission (NE) of the LS sample (light orange) at 515 nm agrees with confocal PL microscope measurements (Figure 2d), and a notably bluer emission was found in BC (light blue, 505 nm), while both in the range of previous reported $(5FPEA)_2PbI_4$.[38,39] The blue-shifted signal of the BC sample also agrees with the absorption spectra. Upon cooling, the NE peak of both samples displayed a narrowing trend (Figure S9), while BC possessed an ∼40 meV bluer peak at all temperatures. After fitting with a Voigt function, the NE full-width-at-half-maximum (fwhm) values are displayed in Figure 4b against temperature. In particular, at low temperatures, the BC sample shows a wider NE peak (24.7 meV at room temperature and 11.3 meV at 4.3 K) with respect to the LS sample. It is important to underline that the detected broadening is most probably the result of a different fine structure (influenced by local disorder and solvent inclusions), which is not resolved in these measurements because of the grating utilized (vide infra).[37]

https://doi.org/10.1021/acsmaterialslett.5c01358
ACS Materials Lett. XXXX, XXX, XXX−XXX

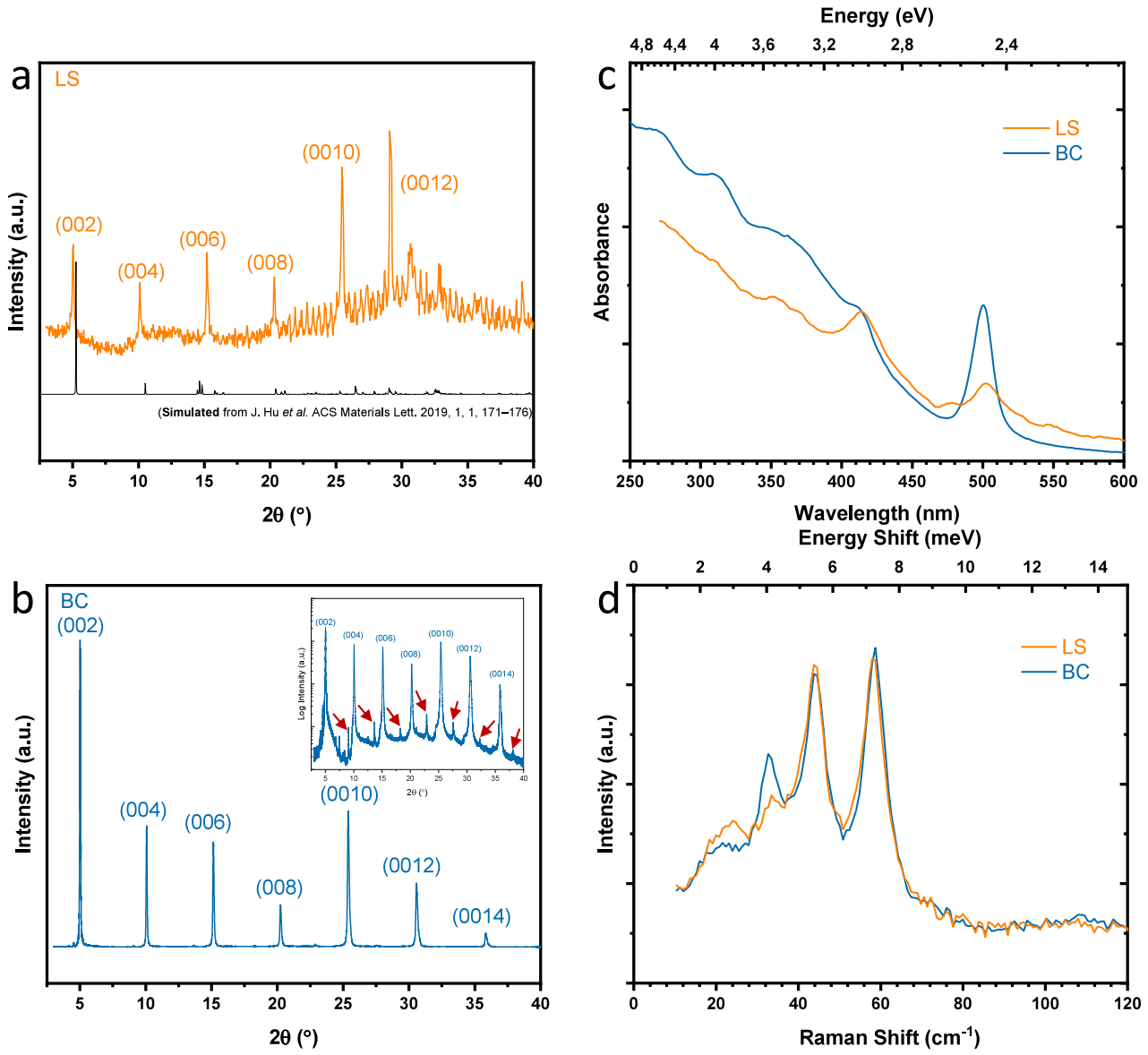

Figure 3. Powder X-ray Diffraction pattern of (a) liquid surface (LS) grown $(5FPEA)_2PbI_4$ sheets and (b) $(5FPEA)_2PbI_4$ blade-coated (BC) thin film. (c) Absorbance spectrum and (d) Raman spectrum of the LS and BC samples.

Based on the XRD results, such a blue-shift and the larger fwhm of the BC sample could be related to the presence of a solvent-intercalated 2D perovskite phase. The larger interlayer separation and different dielectric screening could result in higher energy PL emission, while energy disorders within the film provide additional broadening factors. With its unique fabrication method, the LS samples do not suffer from this issue.

At room temperature, a broad emission (BE) peak around 720 nm can be readily found in the BC sample, which is minimal for LS. The relative intensity of these peaks steadily grew with decreasing temperature, and they became quite dominant when cooled below 70−80 K especially in the LS sample (Figure S9). This behavior has been previously observed for other iodide RP systems and is related to trap states (iodine vacancies), or in certain (chloride or bromide) systems, self-trapped excitons.[29,37,40] In addition, a secondary, more complex broad structure around 600 nm was clearly resolved below 70 K, previously also seen in $(FPEA)_2PbI_4$,[41] reaching its peak relative intensity at 30 K.

Time-resolved PL characteristics of the NE and BE echo previous reports,[37,41] where the lifetime of the NE peak decreases (in the ns regime) and that of the BE peak increases (up to μs) with decreasing temperature (Figure S10a and S10b, respectively), highlighting the complex recombination pathways including energy transfer between free excitons and trapped states. In Figure 4c, the normalized PL decays of the NE of LS and BC at room temperature and 4.3 K are compared. The BC sample showed a slower decay compared to LS. The transients can be fitted with a biexponential model, yielding an average τ of 82 (τ_1 = 61 ps, τ_2 = 312 ps) and 129 ps (τ_1 = 83 ps, τ_2 = 350 ps) for LS and BC, respectively. Overall, benchmarking with blade-coated thin films, the narrow blue emission and comparable decay dynamics of the liquid surface prepared ultrathin perovskite quantum wells showcase their attractive optical properties.

https://doi.org/10.1021/acsmaterialslett.5c01358
ACS Materials Lett. XXXX, XXX, XXX−XXX

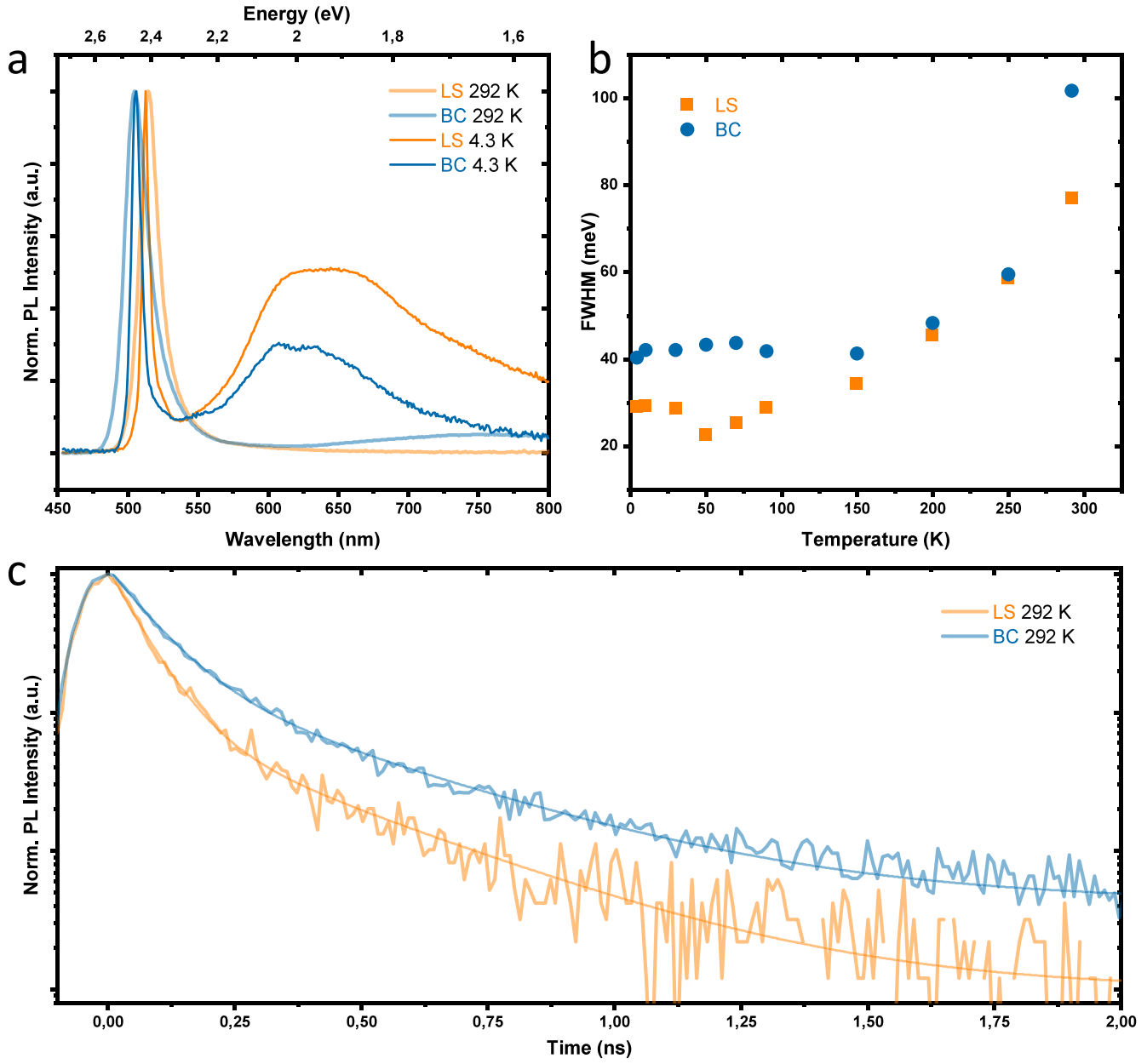

Figure 4. Photoluminescence properties of the liquid surface grown $(5FPEA)_2PbI_4$ sheets (LS, orange) and $(5FPEA)_2PbI_4$ thin film made by blade coating (BC, blue). (a) Steady-state PL spectra at 292 K (light) and 4.3 K (dark color). (b) Full-width-at-half-maximum (fwhm) versus temperature plot of the narrow emission (NE) peak. (c) Time-resolved PL intensity of the NE peak at 292 K for both LS and BC samples.

To summarize, we here introduce a facile liquid surface synthesis method to obtain ultrathin n = 1 RP metal halide perovskite sheets at room temperature, where precursor solutions containing the entire 2D perovskite formulation are spread on an antisolvent substrate. Crucially important is to balance the floating, spreading, and crystallization aspects of the perovskite at the antisolvent−air interface, where liquid phase formulations and related kinetic parameters are optimized. The obtained perovskite thin sheets are on par in geometry with state-of-the-art ultrathin 2D perovskites, and compared to blade-coated thin films of the same chemical composition, the liquid surface grown quantum wells provided analogous or slightly improved light emission quality, possibly due to the absence of remnant solvents. Future studies may include preparing quantum wells with higher n perovskite phases and other chemical compositions, where transfer stacking of 2D materials and device fabrication could follow.

■ ASSOCIATED CONTENT

Data Availability Statement

The data underlying this study is openly available in DataverseNL at https://doi.org/10.34894/7OA35J.

Supporting Information

The Supporting Information is available free of charge at https://pubs.acs.org/doi/10.1021/acsmaterialslett.5c01358.

Experimental and characterization methods, notes on previous thin sheet 2D perovskite synthesis methods, and additional data including microscopic and spectroscopic characterizations of the synthesized perovskite sheets (PDF)

https://doi.org/10.1021/acsmaterialslett.5c01358
ACS Materials Lett. XXXX, XXX, XXX−XXX

AUTHOR INFORMATION

Corresponding Author

Maria Antonietta Loi − *Zernike Institute for Advanced Materials, University of Groningen, Groningen 9747 AG, The Netherlands;* orcid.org/0000-0002-7985-7431; Email: M.A.Loi@rug.nl

Authors

Jiaxiong Li − *Zernike Institute for Advanced Materials, University of Groningen, Groningen 9747 AG, The Netherlands;* orcid.org/0000-0003-3743-1149

Mordechai Kot − *Zernike Institute for Advanced Materials, University of Groningen, Groningen 9747 AG, The Netherlands;* orcid.org/0009-0003-8999-4557

Nina Cielica − *Zernike Institute for Advanced Materials, University of Groningen, Groningen 9747 AG, The Netherlands*

Jacopo Pinna − *Zernike Institute for Advanced Materials, University of Groningen, Groningen 9747 AG, The Netherlands;* orcid.org/0000-0003-1899-0113

Lijun Chen − *Zernike Institute for Advanced Materials, University of Groningen, Groningen 9747 AG, The Netherlands;* orcid.org/0000-0003-4530-2566

Francesco Modena − *Zernike Institute for Advanced Materials, University of Groningen, Groningen 9747 AG, The Netherlands*

Laurence Lutsen − *Energyville, imo-imomec, B-3600 Genk, Belgium; imec, imo-imomec, B-3590 Diepenbeek, Belgium*

Wouter T. M. Van Gompel − *Energyville, imo-imomec, B-3600 Genk, Belgium; imec, imo-imomec, B-3590 Diepenbeek, Belgium; Hasselt University, Institute for Materials Research (imo-imomec), Hybrid Materials Design (HyMaD), B-3500 Hasselt, Belgium;* orcid.org/0000-0002-8173-5206

Complete contact information is available at: https://pubs.acs.org/10.1021/acsmaterialslett.5c01358

Notes

The authors declare no competing financial interest.

ACKNOWLEDGMENTS

The authors would like to express their gratitude to the technical assistance of Arjen Kamp, Teodor Zaharia and Gert ten Brink. Laurence Lutsen and Wouter T. M. Van Gompel thank the Research Foundation Flanders (FWO) for funding through the FWO research project G0A8723N. This work is funded by the European Commission (ERC-AdvancedGrant, DEOM, 101055097). Views and opinions expressed are however those of the author(s) only and do not necessarily reflect those of the European Union or the European Research Council. Neither the European Union nor the granting authority can be held responsible for them.

REFERENCES

(1) Dong, H.; Ran, C.; Gao, W.; Li, M.; Xia, Y.; Huang, W. Metal Halide Perovskite for next-generation optoelectronics: progresses and prospects. *eLight* **2023**, *3* (1), No. 3.

(2) Liu, X. K.; Xu, W.; Bai, S.; Jin, Y.; Wang, J.; Friend, R. H.; Gao, F. Metal halide perovskites for light-emitting diodes. *Nat. Mater.* **2021**, *20* (1), 10−21.

(3) Stranks, S. D.; Snaith, H. J. Metal-halide perovskites for photovoltaic and light-emitting devices. *Nat. Nanotechnol* **2015**, *10* (5), 391−402.

(4) Li, X.; Hoffman, J. M.; Kanatzidis, M. G. The 2D Halide Perovskite Rulebook: How the Spacer Influences Everything from the Structure to Optoelectronic Device Efficiency. *Chem. Rev.* **2021**, *121* (4), 2230−2291.

(5) Mao, L.; Stoumpos, C. C.; Kanatzidis, M. G. Two-Dimensional Hybrid Halide Perovskites: Principles and Promises. *J. Am. Chem. Soc.* **2019**, *141* (3), 1171−1190.

(6) Katan, C.; Mercier, N.; Even, J. Quantum and Dielectric Confinement Effects in Lower-Dimensional Hybrid Perovskite Semiconductors. *Chem. Rev.* **2019**, *119* (5), 3140−3192.

(7) Tan, C.; Chen, J.; Wu, X.-J.; Zhang, H. Epitaxial growth of hybrid nanostructures. *Nature Reviews Materials* **2018**, *3* (2), No. 17089.

(8) Sun, J.; Choi, Y.; Choi, Y. J.; Kim, S.; Park, J. H.; Lee, S.; Cho, J. H. 2D-Organic Hybrid Heterostructures for Optoelectronic Applications. *Adv. Mater.* **2019**, *31* (34), No. e1803831.

(9) Li, R.; Li, L. J.; Cheng, Y.; Huang, W. Recent Advances in van der Waals Heterojunctions Based on Semiconducting Transition Metal Dichalcogenides. *Advanced Electronic Materials* **2018**, *4* (11), No. 1800270.

(10) Lei, Y.; Li, Y.; Lu, C.; Yan, Q.; Wu, Y.; Babbe, F.; Gong, H.; Zhang, S.; Zhou, J.; Wang, R.; et al. Perovskite superlattices with efficient carrier dynamics. *Nature* **2022**, *608* (7922), 317−323.

(11) Gu, H.; Xia, J.; Liang, C.; Chen, Y.; Huang, W.; Xing, G. Phase-pure two-dimensional layered perovskite thin films. *Nature Reviews Materials* **2023**, *8*, 533.

(12) Soe, C. M. M.; Nagabhushana, G. P.; Shivaramaiah, R.; Tsai, H.; Nie, W.; Blancon, J. C.; Melkonyan, F.; Cao, D. H.; Traore, B.; Pedesseau, L.; et al. Structural and thermodynamic limits of layer thickness in 2D halide perovskites. *Proc. Natl. Acad. Sci. U. S. A.* **2019**, *116* (1), 58−66.

(13) Pei, K.; Zhai, T. Emerging 2D Organic-Inorganic Heterojunctions. *Cell Reports Physical Science* **2020**, *1* (8), 100166.

(14) Pham, P. V.; Bodepudi, S. C.; Shehzad, K.; Liu, Y.; Xu, Y.; Yu, B.; Duan, X. 2D Heterostructures for Ubiquitous Electronics and Optoelectronics: Principles, Opportunities, and Challenges. *Chem. Rev.* **2022**, *122* (6), 6514−6613.

(15) Shi, E.; Dou, L. Halide Perovskite Epitaxial Heterostructures. *Accounts of Materials Research* **2020**, *1* (3), 213−224.

(16) Wang, H.; Ma, J.; Li, D. Two-Dimensional Hybrid Perovskite-Based van der Waals Heterostructures. *J. Phys. Chem. Lett.* **2021**, *12* (34), 8178−8187.

(17) Dou, L.; Wong, A. B.; Yu, Y.; Lai, M.; Kornienko, N.; Eaton, S. W.; Fu, A.; Bischak, C. G.; Ma, J.; Ding, T. Atomically thin two-dimensional organic-inorganic hybrid perovskites. *Science* **2015**, *349* (6255), 1518.

(18) Pan, D.; Fu, Y.; Spitha, N.; Zhao, Y.; Roy, C. R.; Morrow, D. J.; Kohler, D. D.; Wright, J. C.; Jin, S. Deterministic fabrication of arbitrary vertical heterostructures of two-dimensional Ruddlesden-Popper halide perovskites. *Nat. Nanotechnol* **2021**, *16* (2), 159−165.

(19) Forlano, K. M.; Roy, C. R.; Mihalyi-Koch, W.; Hossain, T.; Sanders, K.; Guzei, I.; Graham, K. R.; Wright, J. C.; Jin, S. High Layer Number (n = 1−6) 2D Ruddlesden-Popper Lead Bromide Perovskites: Nanosheets, Crystal Structure, and Optoelectronic Properties. *ACS Materials Letters* **2023**, *5* (11), 2913−2921.

(20) Liu, Y.; Ye, H.; Zhang, Y.; Zhao, K.; Yang, Z.; Yuan, Y.; Wu, H.; Zhao, G.; Yang, Z.; Tang, J.; et al. Surface-Tension-Controlled Crystallization for High-Quality 2D Perovskite Single Crystals for Ultrahigh Photodetection. *Matter* **2019**, *1* (2), 465−480.

(21) Zhumekenov, A. A.; Burlakov, V. M.; Saidaminov, M. I.; Alofi, A.; Haque, M. A.; Turedi, B.; Davaasuren, B.; Dursun, I.; Cho, N.; El-Zohry, A. M.; et al. The Role of Surface Tension in the Crystallization of Metal Halide Perovskites. *ACS Energy Letters* **2017**, *2* (8), 1782−1788.

(22) Tutantsev, A. S.; Udalova, N. N.; Fateev, S. A.; Petrov, A. A.; Chengyuan, W.; Maksimov, E. G.; Goodilin, E. A.; Tarasov, A. B. New Pigeonholing Approach for Selection of Solvents Relevant to Lead Halide Perovskite Processing. *J. Phys. Chem. C* **2020**, *124* (20), 11117−11123.

(23) Sidhik, S.; Wang, Y.; De Siena, M.; Asadpour, R.; Torma, A. J.; Terlier, T.; Ho, K.; Li, W.; Puthirath, A. B.; Shuai, X.; et al. Deterministic fabrication of 3D/2D perovskite bilayer stacks for durable and efficient solar cells. *Science* **2022**, *377* (6613), 1425−1430.
(24) Wu, C.; Wang, K.; Li, J.; Liang, Z.; Li, J.; Li, W.; Zhao, L.; Chi, B.; Wang, S. Volatile solution: the way toward scalable fabrication of perovskite solar cells? *Matter* **2021**, *4* (3), 775−793.
(25) Li, B.; Li, J.; Ni, D.; Tang, S.; Fan, J.; Shi, K.; Li, Z.; Zhou, J. Spontaneously spread polymer thin films on the miscible liquid substrates. *Chemical Engineering Journal* **2022**, *437*, 135443.
(26) Large, M. J.; Ogilvie, S. P.; King, A. A. K.; Dalton, A. B. Understanding Solvent Spreading for Langmuir Deposition of Nanomaterial Films: A Hansen Solubility Parameter Approach. *Langmuir* **2017**, *33* (51), 14766−14771.
(27) Lee, Y. H.; Park, J. Y.; Niu, P.; Yang, H.; Sun, D.; Huang, L.; Mei, J.; Dou, L. One-Step Solution Patterning for Two-Dimensional Perovskite Nanoplate Arrays. *ACS Nano* **2023**, *17* (14), 13840−13850.
(28) Kim, S. Y.; Yang, J. M.; Choi, E. S.; Park, N. G. Effect of interlayer spacing in layered perovskites on resistive switching memory. *Nanoscale* **2019**, *11* (30), 14330−14338.
(29) Du, K.-z.; Tu, Q.; Zhang, X.; Han, Q.; Liu, J.; Zauscher, S.; Mitzi, D. B. Two-Dimensional Lead(II) Halide-Based Hybrid Perovskites Templated by Acene Alkylamines: Crystal Structures, Optical Properties, and Piezoelectricity. *Inorg. Chem.* **2017**, *56* (15), 9291−9302.
(30) Ye, J. Y.; Tong, J.; Hu, J.; Xiao, C.; Lu, H.; Dunfield, S. P.; Kim, D. H.; Chen, X.; Larson, B. W.; Hao, J. Enhancing Charge Transport of 2D Perovskite Passivation Agent for Wide-Bandgap Perovskite Solar Cells Beyond 21%. *Solar RRL* **2020**, *4* (6), No. 2000082.
(31) Hu, J.; Oswald, I. W. H.; Hu, H.; Stuard, S. J.; Nahid, M. M.; Yan, L.; Chen, Z.; Ade, H.; Neilson, J. R.; You, W. Aryl-Perfluoroaryl Interaction in Two-Dimensional Organic-Inorganic Hybrid Perovskites Boosts Stability and Photovoltaic Efficiency. *ACS Materials Letters* **2019**, *1* (1), 171−176.
(32) Zhuang, Y.; Ma, P.; Shi, J.; Lin, H.; You, G.; Xu, G.; Cai, B. Stability Improvement of 2D Perovskite by Fluorinated-Insulator. *Advanced Materials Interfaces* **2021**, *8* (20), No. 2101343.
(33) Mitzi, D. B.; Medeiros, D. R.; Malenfant, P. R. L. Intercalated organic inorganic perovskites stabilized by fluoroaryl aryl interactions. *Inorg. Chem.* **2002**, *41* (8), 2134−2145.
(34) Mitzi, D. B.; Medeiros, D. R.; DeHaven, P. W. Low temperature melt processing of organic inorganic hybrid films. *Chem. Mater.* **2002**, *14* (7), 2839−2841.
(35) Van Gompel, W. T. M.; Herckens, R.; Van Hecke, K.; Ruttens, B.; D'Haen, J.; Lutsen, L.; Vanderzande, D. Low-Dimensional Hybrid Perovskites Containing an Organic Cation with an Extended Conjugated System: Tuning the Excitonic Absorption Features. *ChemNanoMat* **2019**, *5* (3), 323−327.
(36) Scalon, L.; Brunner, J.; Guaita, M. G. D.; Szostak, R.; Albaladejo-Siguan, M.; Kodalle, T.; Guerrero-León, L. A.; Sutter-Fella, C. M.; Oliveira, C. C.; Vaynzof, Y. Tuning Phase Purity in Chiral 2D Perovskites. *Advanced Optical Materials* **2024**, *12* (2), No. 2300776.
(37) Tekelenburg, E. K.; Kahmann, S.; Kamminga, M. E.; Blake, G. R.; Loi, M. A. Elucidating the Structure and Photophysics of Layered Perovskites through Cation Fluorination. *Advanced Optical Materials* **2021**, *9* (18), No. 2001647.
(38) Wei, Y.; Audebert, P.; Galmiche, L.; Lauret, J. S.; Deleporte, E. Synthesis, optical properties and photostability of novel fluorinated organic-inorganic hybrid (R-NH3)2PbX4 semiconductors. *J. Phys. D: Appl. Phys.* **2013**, *46* (13), 135105.
(39) Lekina, Y.; Han, M.; Febriansyah, B.; Li, Y.; Nguyen, T. T.; Shen, Z. X. Ordering and Disordering Dynamics in Fluorinated Two Dimensional Perovskites under High Pressure. *Chem. Mater.* **2025**, *37* (15), 5569−5580.
(40) Kahmann, S.; Meggiolaro, D.; Gregori, L.; Tekelenburg, E. K.; Pitaro, M.; Stranks, S. D.; De Angelis, F.; Loi, M. A. The Origin of Broad Emission in ⟨100⟩ Two-Dimensional Perovskites: Extrinsic vs Intrinsic Processes. *ACS Energy Lett.* **2022**, *7* (12), 4232−4241.
(41) Kahmann, S.; Tekelenburg, E. K.; Duim, H.; Kamminga, M. E.; Loi, M. A. Extrinsic nature of the broad photoluminescence in lead iodide-based Ruddlesden-Popper perovskites. *Nat. Commun.* **2020**, *11* (1), 2344.

https://doi.org/10.1021/acsmaterialslett.5c01358
ACS Materials Lett. XXXX, XXX, XXX−XXX